Invited Paper

Optimizing doubly-resonant photonic crystal cavity modes for second harmonic generation

Momchil Minkov[a] and Vincenzo Savona[a]

[a]Institute of Theoretical Physics, Ecole Polytechnique Fdrale de Lausanne EPFL, CH-1015 Lausanne, Switzerland

ABSTRACT

We optimize a photonic crystal slab for the generation of second harmonic. The optimization consists in two steps. In the first step a regular photonic crystal, consisting in a triangular lattice of circular holes in a dielectric slab, is optimized by allowing for holes of three alternating radii, with the objective of obtaining a high-frequency bandgap doubly resonant with the fundamental one. The second step consists in modeling a L3 defect cavity in such a photonic crystal where, by further varying the radii and positions of a few neighboring holes, doubly resonant modes at the fundamental and second harmonic frequencies are obtained, with maximal Q-factors and field overlap. The structure emerging from this optimization procedure has Q-factors of 3400 for the fundamental mode and of 430 for the doubly resonant one. Due to the localized nature of those modes and hence their large field overlap, efficient second-harmonic generation is expected in a material with a $\chi^{(2)}$ non-linearity.

Keywords: Photonic crystal, microcavity, second harmonic generation

1. INTRODUCTION

Second harmonic generation (SHG) is a second-order nonlinear process that achieves frequency conversion of light. Efficient frequency conversion devices, integrated in a nanophotonic platform, are highly needed for several applications, spanning from classical and quantum light sources, to interfacing devices operating at different frequencies in a quantum optical network in view of photon-based quantum information processing. The intrinsic nonlinearity of materials commonly used for applications in integrated optics is generally very weak, thus requiring long interaction lengths and times and/or strong power of the input field, in order to make the conversion process efficient.

In order to conceive SHG devices suitable for a nanophotonic platform, the efficiency of the SHG process can be drastically enhanced in resonant structures such as high-Q cavities and waveguides. The enhancement in the waveguide scheme arises from the slow-light propagation – alternatively explained as a local spectral increase in the density of optical modes – in devices with appropriately engineered dispersion, like e.g. in coupled optical resonator waveguides. In optical cavities on the other hand, SHG enhancement originates from the high Q-factor and small modal volume, respectively increasing the interaction time and field intensity. More specifically however, the SHG enhancement in an optical cavity will rely on the existence of a double optical resonance – at the fundamental and second harmonic frequencies – and on a significant spatial overlap of these two modes. The enhancement factor in particular is proportional to a mode overlap factor and to the product $Q_1^2 Q_2$, where Q_1 and Q_2 are the Q-factors of the fundamental and second harmonic modes respectively.[1] The main challenge in the design of an efficient SHG caviy device is thus to engineer a doubly resonant optical resonator – i.e. having two resonant modes at the fundamental and SHG frequencies – with the highest Q-factors at both frequencies.

SHG microphotonic devices with high efficiency have been realized with various device geometries, including microdisks and microrings,[2–5] waveguides,[4,6–8] and nanobeam cavities,[9–11] using various semiconductor materials. In these cases, the geometry of the devices was optimized to accommodate doubly resonant modes. It would be desirable to achieve the doubly resonant condition for a defect cavity in a photonic crystal slab.[1] With respect to other geometries in fact, the photonic crystal slab paradigm presents several advantages, in particular in terms of ease of integration, scalability, and the possibility to realize various cavity designs with high Q-factors

Send correspondence to: M.M. e-mail: momchil.minkov@epfl.ch; V.S. e-mail: vincenzo.savona@epfl.ch

Photonic Crystal Materials and Devices XI, edited by Sergei G. Romanov, Gabriel Lozano, Dario Gerace, Christelle Monat, Hernán Ruy Míguez, Proc. of SPIE Vol. 9127, 91270C
 · doi: 10.1117/12.2058987

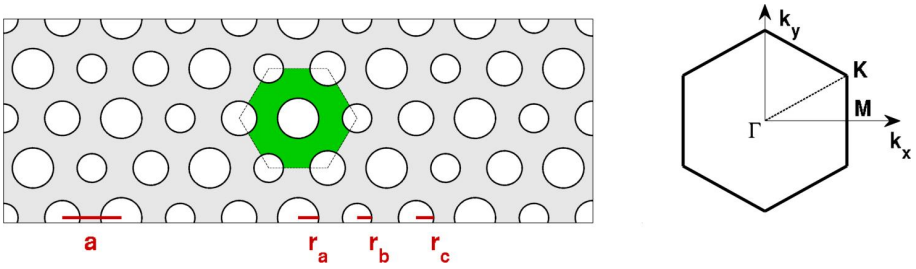

Figure 1. The PhC studied here with a triangular lattice of pitch a of circular holes of three different radii, r_a, r_b and r_c. One choice of the elementary cell as well as the first Brillouin zone in reciprocal space are also shown.

and ultrasmall mode volumes. Several works have recently achieved SHG in photonic crystal slab cavities.[1,12–16] However, to the best of our knowledge, a doubly resonant design for this system is still lacking.

Here, we combine a fast simulation tool for photonic crystal cavities – the guided-mode expansion (GME) method[17] – to a global optimization algorithm, making it possible to explore a large space of structural variations. Using GME, we derive an optimal design for the triangular lattice of circular holes displaying doubly resonant photonic bandgaps (i.e. where the frequency range of the second bandgap, when halved, overlaps with the fundamental bandgap). Then, starting from this photonic crystal design and using GME combined with global optimization, we derive an optimal design for the L3 cavity, which has a double resonance with high Q-factors and large mode overlap. If fabricated, this cavity design would bring a significant improvement to the SHG efficiency achieved in state-of-the-art photonic crystal slab devices, thus opening the way to novel quantum devices.[18,19]

2. COMPUTATIONAL PARAMETERS

The starting point of this work is a photonic crystal formed by a triangular lattice of circular holes etched in a dielectric slab (Fig. 1). Since all quantities scale with the lattice constant a, the choice of units here is $[a]$ for lengths, $[1/a]$ for wave-vectors, and $[2\pi c/a]$ for frequencies, and we set the slab thickness everywhere to $d = 0.5a$. Contrary to the standard structure with a constant hole radius, however, here we allow for three different, alternating hole radii: r_a, r_b and r_c in Fig. 1. The structure can thus be viewed as three superimposed lattices of pitch $\sqrt{3}a$ rotated at 60° from one another, each with holes of a constant radius (the widely-used constant-radius PhC is thus obtained when $r_a = r_b = r_c = r$). The smallest elementary cell of the crystal (green hexagon in Fig. 1) contains three holes, one of each kind, and the first Brillouin zone of the lattice is a hexagon in k-space with three symmetry points, Γ, M and K. Notice that the structure is symmetric under exchange of any of the three radii, and although below we always have r_a as the largest, the choice is completely arbitrary. Since the PhC is symmetric with respect to the plane bisecting the slab in the x-y direction, its modes are split into even ($\hat{\sigma}_{xy} = 1$) and odd ($\hat{\sigma}_{xy} = -1$) with respect to the mirror reflection operator ($\hat{\sigma}$). In a linear-optical crystal, those even and odd modes are completely decoupled, but in the presence of a non-linear response, they can be mixed. In Ref. 17 it was shown that in a triangular lattice of *triangular* holes, a band-gap in the dispersion of the $\hat{\sigma}_{xy} = -1$ modes exists around twice the central frequency of the fundamental band-gap of the $\hat{\sigma}_{xy} = 1$ modes. Triangular holes are, however, challenging to fabricate, which is what ultimately motivates the present study using circular holes. Note that positive x-y-reflection symmetry imposes $E_z = 0$ in the center of the slab for the $\hat{\sigma}_{xy} = 1$ modes, while in the negative-symmetry case the opposite is true: $E_x = E_y = 0$, and only E_z remains in the slab center. The doubly-resonant modes will thus interact the most in the presence of a non-isotropic susceptibility tensor that couples E_x and E_y of one mode to E_z of another.[20]

The numerical tool used here is the GME of Ref. 17, in which the Bloch modes of the PhC are expanded on the basis of the guided modes of an effective dielectric slab (without the holes). Apart from simulating a regular PhC, this method is also reliable for simulating point and line defects (cavities and waveguides), in which case the computational space is a large enough *super*cell that includes the defect. In addition to resonant frequencies, losses (quality factors Q) can also be reliably computed in a Fermi-golden-rule fashion.[17,21] Here, we choose GaAs as the slab material due to its strong non-linear response and the fact that it is widely used in the PhC domain, and we set the target wavelength of operation to ≈ 1750nm for the first-order modes and correspondingly

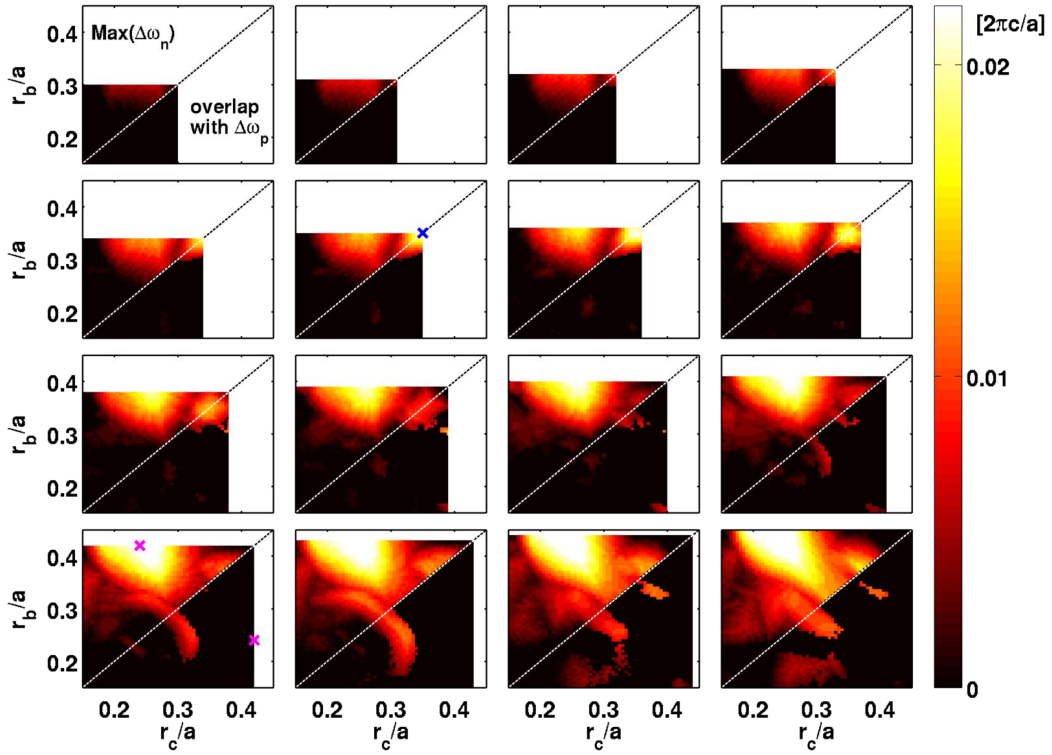

Figure 2. Width of the negative-symmetry band-gap and its overlap with twice the positive-symmetry one, as a function of r_a (starting from $0.3a$ in the first panel, and increasing in steps of $0.01a$ up to $0.45a$ in the last one), r_b (on the y-axis of each panel) and r_c (on the x-axis of each panel); r_b and r_c go only up to the corresponding r_a. The symmetry upon exchange of r_b and r_c translates in a symmetry under reflection along the $r_b = r_c$ diagonal in each panel (marked with a dashed line). Above this diagonal, the maximum width of the negative-symmetry band-gap is plotted. For the equivalent points below, the amount of overlap with the positive-symmetry band-gap is shown, all in units of $2\pi c/a$.

$\approx$ 875nm for the second-order ones (i.e. at energy slightly lower than the width of the electronic band-gap at room temperature). The choice of these particular values is only needed to determine the refractive index of the slab. Since material dispersion is not taken into account in the GME, we set the refractive index to 3.362 for all positive-symmetry computations and to 3.566 for all negative-symmetry ones, so that the precision is the highest in the corresponding target frequency ranges. The reciprocal-space vectors $\mathbf{G}$ included in the computation are truncated to $G_{\max} = 3\frac{2\pi}{a}$ everywhere, while respectively 2 and 3 guided modes were used in the $\hat{\sigma}_{xy} = 1$ and $\hat{\sigma}_{xy} = -1$ computations (convergence vs. those parameters was thoroughly checked).

3. RESULTS

3.1 Regular crystal band structure

The positive-symmetry modes present a broad band-gap for any choice of r_a, r_b and r_c in the range $[0.15a \dots 0.45a]$. For a given set of r_a, r_b and r_c, we denote this gap by its two frequency boundaries $\boldsymbol{\omega}_p = (\omega_p^{(1)}, \omega_p^{(2)})$. The aim of this study is then to find a configuration of radii for which a negative-symmetry gap $\boldsymbol{\omega}_n$ is also present, such as $\boldsymbol{\omega}_n/2$ overlaps with $\boldsymbol{\omega}_p$, and is as broad as possible. As a first step, we compute the positive- and negative-symmetry density of states of the crystal as a function of r_a r_b and r_c, in the range $r_a = [0.3a \dots 0.45a]$, $r_b = [0.15a \dots r_a]$, $r_c = [0.15a \dots r_b]$. All configurations can be obtained by these ones upon permutation of the three radii. The search for the best configuration is then summarized in Fig. 2, where in each panel r_b and r_c are plotted along the vertical and horizontal axes, respectively, while r_a increases across panels in units of $0.01a$, starting from $0.3a$. In each panel, above the $r_b = r_c$ diagonal (dashed line), the maximum width of the negative-symmetry band-gap $\Delta\boldsymbol{\omega}_n = \omega_n^{(2)} - \omega_n^{(1)}$ is shown ('maximum' in case that more than one gaps are

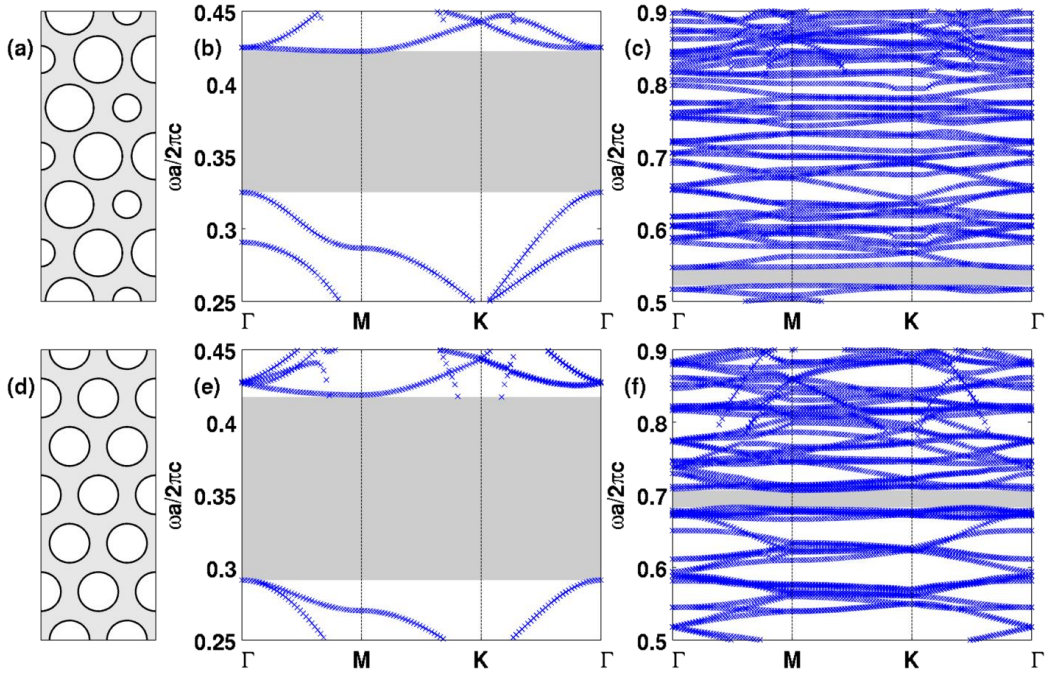

Figure 3. Top panels: (a): PhC with $r_a = r_b = 0.42a$, $r_c = 0.24a$. The band diagrams for (b): the positive-symmetry modes and (c): the negative-symmetry modes at twice the frequency are shown. Band-gaps are shaded in grey. (d)-(f): same, but for the $r_a = r_b = r_c = 0.35a$ configuration.

present). Simultaneously, for the same points (due to the symmetry under exchange of r_b and r_c), below the diagonal we show the overlap of this band-gap with $\boldsymbol{\omega}_p$. We are then looking for a configuration with a high value both above and below the diagonal.

In terms of gap-width, we see two main regions where a negative-symmetry gap broader than $0.02\frac{2\pi c}{a}$ exists. However, only in one of the two cases does $\boldsymbol{\omega}_n$ also *overlap* with the positive-symmetry gap. The band diagrams for two representative configurations are shown in Fig. 3. The first (panel (a)) has $r_a = 0.42a$, $r_b = 0.42a$, $r_c = 0.24a$ (magenta crosses in Fig. 2). In panel (b), we show the positive-symmetry band-diagram, while in panel (c): the negative-symmetry one at twice the frequency. The band-gaps are shaded in grey, and as could be also inferred from Fig. 2, a relatively broad $\hat{\sigma}_{xy} = -1$ band-gap is present, but it does not overlap with the $\hat{\sigma}_{xy} = 1$ one ($\boldsymbol{\omega}_n$ is too low). The second configuration (Fig. 3(d)-(f)) has $r_a = r_b = r_c = 0.35a$ (blue cross in Fig. 2), and in this case, the positive-symmetry gap (grey area in (e)) is doubly-resonant with the negative-symmetry one (grey area in (f)). In addition, $\boldsymbol{\omega}_n$ is just as broad as in panel (c). Thus, the best configuration in the r_a-r_b-r_c type of PhC considered here turns out to be the standard r-r-r crystal with $r = 0.35a$.

3.2 Doubly-resonant L3 cavity modes

Next, to increase the strength of the non-linear interaction, we consider a defect cavity in the regular PhC lattice with $r = 0.35a$. We choose the widely-used L3 design[22] formed by removing 3 holes in a line. The mode structure of this cavity is summarized in Fig. 4. In panel (a) we plot with blue crosses the frequencies of the localized positive-symmetry modes, and with red crosses the halved frequencies of the localized negative-symmetry modes. Since the $\boldsymbol{\omega}_n$ gap is narrow, there are many modes inside it, close in frequency to one another. In the zoomed-in region it can also be seen that one of the positive-symmetry modes is doubly resonant with the negative-symmetry band-gap. In panel (b), we plot the electric field distribution in the cavity for the eight $\hat{\sigma}_{xy} = 1$ modes, while in panel (c), we show all seventeen of the $\hat{\sigma}_{xy} = -1$ modes.

From Fig. 4 it appears clearly that one of the positive-symmetry modes is close to doubly-resonant with a few negative-symmetry modes. In addition, since the modes of both symmetries are localized in the cavity defect, the field overlap is high and the non-linear interaction is expected to be much stronger than for modes in the

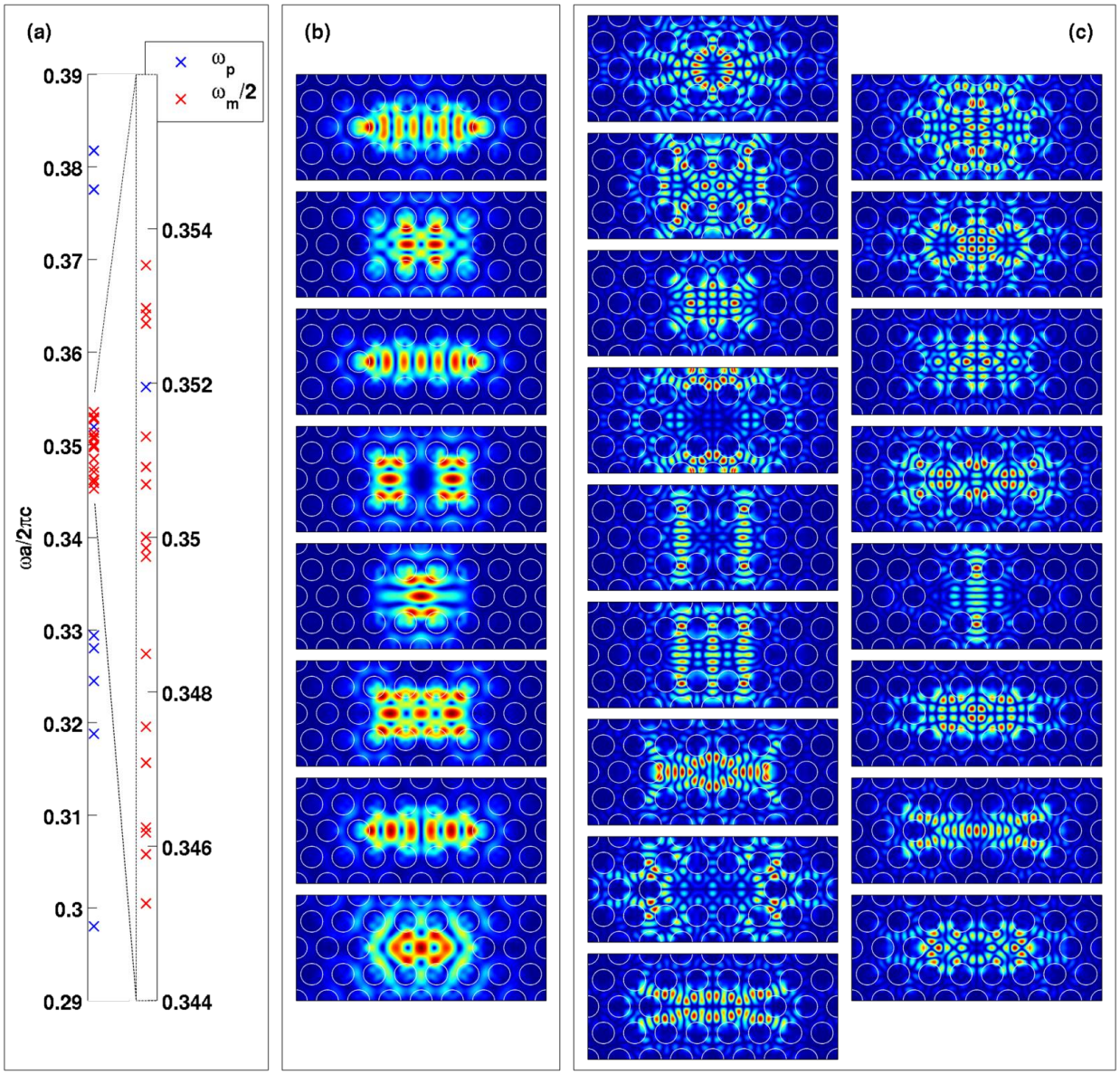

Figure 4. Resonant modes of the L3 cavity. (a) The frequencies of the positive-symmetry (blue) and negative-symmetry (red, divided by two) localized modes; (b) Electric field ($\sqrt{|E_x|^2 + |E_y|^2}$) profiles in the center of the slab of the positive-symmetry resonant modes; (c) Electric field ($|E_z|$) profiles in the center of the slab of the negative-symmetry resonant modes. In both (b) and (c), the frequency of the corresponding modes increases from bottom to top.

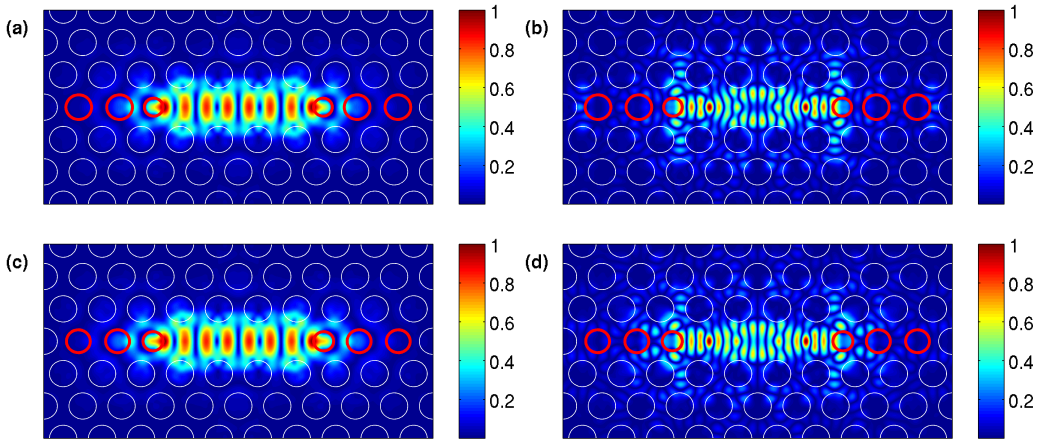

Figure 5. Normalized electric field profiles for the two optimized L3 cavities. (a)-(b): The positive-symmetry (a) and highest-Q negative-symmetry (b) mode of the cavity optimized for highest $Q_p\max(Q_n)$. (c)-(d): The positive-symmetry (c) and highest-Q negative-symmetry (d) mode of the cavity optimized for highest $\max(Q_n)$.

bulk crystal, or in the case in which only the fundamental-frequency mode is confined.[14] However, the modes are quite lossy: the highest positive-symmetry Q is observed for the lowest-frequency mode, which has $Q = 4300$, while the mode which is in the doubly-resonant band-gap has a Q of only 310. The negative-symmetry modes radiate even more strongly: most of the Qs are below 100, and the highest is 110. These fast decay rates set a severe limitation on the applicability of the SHG process. It is known, however, that small variation in a few structural parameters of a PhC cavity can bring about tremendous improvement in quality factor.[23,24] Thus, as a next step, we attempt an optimization of the quality factor Q_p of the $\hat{\sigma}_{xy} = 1$ mode which lies in the negative-symmetry gap together with the quality factors Q_n of (at least one of the) negative-symmetry modes.

To perform the optimization, we vary six structural parameters (Fig. 5): shifts in the x-positions and in the radius of the three holes on each side of the cavity (marked in red in the Figure), and use the genetic optimization provided in the Matlab Global Optimization Toolbox.[25] First, we use the product $Q_p\max(Q_n)$ as an objective function. The optimization results in a shift of the three holes away from the cavity by $0.174a$, $0.050a$, and $0.098a$, respectively, and a decrease in radius of those holes by $0.111a$, $0.021a$, and $0.021a$, respectively (Fig. 5(a)-(b)). The Q_p of this optimized-L3 cavity is 4800 (more than an order of magnitude larger than the Q of the corresponding mode in the starting structure), while the mode with highest Q_n (panel (b)) has $Q_n = 300$, which is a good improvement albeit still low. The modes are found at frequencies $\frac{\omega_p a}{2\pi c} = 0.350$ and $\frac{\omega_m}{2}\frac{a}{2\pi c} = 0.343$, respectively. To try and increase Q_n even further, we run a second optimization with only $\max(Q_n)$ as an objective function, which results in a configuration with shifts $0.110a$, $0.067a$, and $0.074a$, respectively, and radius shrinkage by $0.124a$, $0.016a$, and $0.068a$, respectively (Fig. 5(c)-(d)). This structure has $Q_p = 3400$ and a maximum Q_n (achieved for the mode shown in panel (d)) of 430, with corresponding mode frequencies $\frac{\omega_p a}{2\pi c} = 0.349$ and $\frac{\omega_m}{2}\frac{a}{2\pi c} = 0.343$.

4. DISCUSSION AND OUTLOOK

We have shown an easy-to-fabricate photonic lattice in a dielectric slab that presents a doubly resonant band-gap, an important step towards double-resonance SHG in a two-dimensional PhC. We examine an L3 cavity in this lattice and optimize the structure so that the quality factor of the positive-symmetry mode inside the doubly-resonant band gap is an order of magnitude higher as compared to the unmodified structure, which in addition comes with an increase by a factor of 4 in the Q of the highest-Q negative-symmetry mode. The low volume and high field overlap of the resonant modes is expected to strongly enhance the efficiency of the SHG. While the Qs were significantly improved with respect to an unmodified L3, they are still in the low-to-moderate range typically obtained in a PhC platform. We believe that both values can be improved further, by considering

variations in more structural parameters and/or cavity designs other than the L3; this is left for a further investigation. There is also a technical detail worth mentioning: while convergence of the simulation versus various parameters was checked, there is one whose role is non-trivial. Namely, the effective slab permittivity $\bar{\varepsilon}$ for the computation of the guided modes was taken as an averaged value over the slab geometry, as prescribed in Ref. 17. While the computed PhC modes do not depend strongly on this particular choice, the cutoff frequency at which higher-order guided modes appear, does. These higher-order modes translate into the bands starting at a finite k, visible in panels (b), (c), (e) and (f) of Fig. 3. With increasing $\bar{\varepsilon}$, the cutoff frequency decreases, and those bands penetrate the band gap(s), potentially decreasing the cavity Qs (although, the localized cavity modes are mostly composed of first-order guided modes and thus the effect on Q of the higher-order bands is expected to be small). The physical $\bar{\varepsilon}$ lies somewhere between the averaged permittivity and the permittivity of the dielectric, and can be found e.g. through a first-principle simulation like a Finite-Difference Time-Domain solver. Examining this detail is thus left as an immediate extension to this work. Finally, we also note that we kept $d = 0.5a$ everywhere, while in practice this parameter can also be varied and has a non-trivial effect (with potential benefits). This deserves investigation and is also left to be studied in the next future.

The L3 cavity presented here is the first doubly-resonant two-dimensional PhC structure and is an important step towards realizing highly-efficient SHG in this platform, which is bound to find a variety in applications. While some challenges remain, in particular with respect to further improvement of the quality factors of the resonant modes, there are also plenty of possibilities for improvement that are yet to be explored.

ACKNOWLEDGMENTS

This work was supported by the Swiss National Science Foundation through Project No. 200020_149537. The authors would like to thank Dario Gerace for fruitful suggestions and discussions.

REFERENCES

[1] Buckley, S., Radulaski, M., Petykiewicz, J., Lagoudakis, K. G., Kang, J.-H., Brongersma, M., Biermann, K., and Vuckovic, J., "Below-bandgap second harmonic generation in GaAs photonic crystal cavites in (111)B and (001) crystal orientations," *arXiv:1402.3739 [physics]* (Feb. 2014).

[2] Levy, J. S., Foster, M. A., Gaeta, A. L., and Lipson, M., "Harmonic generation in silicon nitride ring resonators," *Opt. Express* **19**, 11415–11421 (June 2011).

[3] Xiong, C., Pernice, W., Ryu, K. K., Schuck, C., Fong, K. Y., Palacios, T., and Tang, H. X., "Integrated GaN photonic circuits on silicon (100) for second harmonic generation," *Opt. Express* **19**, 10462–10470 (May 2011).

[4] Pernice, W. H. P., Xiong, C., Schuck, C., and Tang, H. X., "Second harmonic generation in phase matched aluminum nitride waveguides and micro-ring resonators," *Applied Physics Letters* **100**, 223501 (May 2012).

[5] Kuo, P. S., Bravo-Abad, J., and Solomon, G. S., "Second-harmonic generation using -quasi-phasematching in a GaAs whispering-gallery-mode microcavity," *Nat Commun* **5** (Jan. 2014).

[6] Xu, Y., Lee, R. K., and Yariv, A., "Propagation and second-harmonic generation of electromagnetic waves in a coupled-resonator optical waveguide," *Journal of the Optical Society of America B* **17**(3), 387 (2000).

[7] Dumeige, Y., "Quasi-phase-matching and second-harmonic generation enhancement in a semiconductor microresonator array using slow-light effects," *Phys. Rev. A* **83**, 045802 (Apr. 2011).

[8] Rivoire, K., Buckley, S., Hatami, F., and Vukovi, J., "Second harmonic generation in GaP photonic crystal waveguides," *Applied Physics Letters* **98**, 263113 (July 2011).

[9] Burgess, I. B., Zhang, Y., McCutcheon, M. W., Rodriguez, A. W., Bravo-Abad, J., Johnson, S. G., and Loncar, M., "Design of an efficient terahertz sourceusing triply resonant nonlinearphotonic crystal cavities," *Opt. Express* **17**, 20099–20108 (Oct. 2009).

[10] Zhang, Y., McCutcheon, M. W., Burgess, I. B., and Loncar, M., "Ultra-high-q TE/TM dual-polarized photonic crystal nanocavities," *Opt. Lett.* **34**, 2694–2696 (Sept. 2009).

[11] Rivoire, K., Buckley, S., and Vukovi, J., "Multiply resonant high quality photonic crystal nanocavities," *Applied Physics Letters* **99**, 013114 (July 2011).

[12] McCutcheon, M. W., Young, J. F., Rieger, G. W., Dalacu, D., Frdrick, S., Poole, P. J., and Williams, R. L., "Experimental demonstration of second-order processes in photonic crystal microcavities at submilliwatt excitation powers," *Phys. Rev. B* **76**, 245104 (Dec. 2007).

[13] Rivoire, K., Lin, Z., Hatami, F., Masselink, W. T., and Vu?kovi?, J., "Second harmonic generation in gallium phosphide photonic crystal nanocavities with ultralow continuous wave pump power," *Opt. Express* **17**, 22609–22615 (Dec. 2009).

[14] Buckley, S., Radulaski, M., Biermann, K., and Vukovi, J., "Second harmonic generation in photonic crystal cavities in (111)-oriented GaAs," *Applied Physics Letters* **103**, 211117 (Nov. 2013).

[15] Diziain, S., Geiss, R., Zilk, M., Schrempel, F., Kley, E.-B., Tnnermann, A., and Pertsch, T., "Second harmonic generation in free-standing lithium niobate photonic crystal l3 cavity," *Applied Physics Letters* **103**, 051117 (Aug. 2013).

[16] Ota, Y., Watanabe, K., Iwamoto, S., and Arakawa, Y., "Nanocavity-based self-frequency conversion laser," *Opt. Express* **21**, 19778–19789 (Aug. 2013).

[17] Andreani, L. C. and Gerace, D., "Photonic-crystal slabs with a triangular lattice of triangular holes investigated using a guied-mode expansion method," *Phys. Rev. B* **73**, 235114 (2006).

[18] Majumdar, A. and Gerace, D., "Single-photon blockade in doubly resonant nanocavities with second-order nonlinearity," *Physical Review B* **87**, 235319 (Jun 2013).

[19] Gerace, D. and Savona, V., "Unconventional photon blockade in doubly resonant microcavities with second-order nonlinearity," *arXiv:1402.4587 [cond-mat, physics:physics, physics:quant-ph]* (Feb 2014).

[20] Sipe, J. E., Moss, D. J., and van Driel, H. M., "Phenomenological theory of optical second- and third-harmonic generation from cubic centrosymmetric crystals," *Phys. Rev. B* **35**, 1129–1141 (Jan 1987).

[21] Minkov, M., Dharanipathy, U. P., Houdré, R., and Savona, V., "Statistics of the disorder-induced losses of high-q photonic crystal cavities," *Opt. Express* **21**, 28233–28245 (Nov 2013).

[22] Akahane, Y., Asano, T., Song, B., and Noda, S., "High-q photonic nanocavity in a two-dimensional photonic crystal," *Nature* **425**, 944–947 (Oct. 2003).

[23] Akahane, Y., Asano, T., Song, B.-S., and Noda, S., "Fine-tuned high-q photonic-crystal nanocavity," *Opt. Express* **13**, 1202–1214 (Feb. 2005).

[24] Dharanipathy, U. P., Minkov, M., Tonin, M., Savona, V., and Houdré, R., "Evolutionarily optimized ultrahigh-q photonic crystal nanocavity," *arXiv:1311.0997 [cond-mat, physics:physics]* (Nov. 2013).

[25] "MATLAB and Global Optimization Toolbox Release 2012b, The MathWorks, Inc., Natick, Massachusetts, United States.."